Progress In Electromagnetics Research C, Vol. 68, 95–106, 2016

Design of Compact Multiband Antenna with Band-Rejection Features for Mobile Broadband Satellite Communications

Lamyae Akrou[1, 2, *], Otman Aghzout[3], Henrique Silva[2], and Mohamed Essaaidi[4]

Abstract—This paper presents the design of a compact printed multi-band antenna for satellite communications within vehicular applications. The designed antenna is characterized by its compact size of 24 mm × 18 mm and multiple resonances over WiMAX, WLAN, 5 GHz U-NII, C-band, X-band, Ku-band, K-band and Ka-band. The performance of the multi-band antenna is investigated, and its equivalent circuit model is presented. Good performance is achieved over all the operating bands, with a relatively high gain and efficiency. Furthermore, as the interference with coexisting wireless systems can have a severe impact on the performance of the antenna, four variants of the antenna are proposed incorporating band rejection features within the antenna design. Embedded quarter-wavelength spur-lines, slots, and parasitic elements were used.

1. INTRODUCTION

Nowadays, the need to incorporate broadband services in moving vehicles has drastically increased. Constrained by aesthetic requirements of the vehicles industry, the printed antennas are considered as the most adequate candidate to meet the market demands, due to their ease of fabrication, low production cost, light weight and robustness [1, 2]. Presently, microstrip antennas (MSA) are used in several application, starting from small electronic devices for radio communication to aircraft, spacecraft and satellite communication systems. Moreover, multi-band printed antennas present an intrinsic property for the vehicles, as they permit reducing the amount of integrated antennas in each vehicle. On the other side, printed antennas with band notched functionality have been broadly investigated, with a main focus was on the ultra-wideband antennas (UWB) [3–5], as they tend to lower electromagnetic interference between the operating bands,in order to improve the antenna performance. In [6–8], the authors obtained the band notched function by incorporating a pair of slots on the antenna. In [9] and [10] the use of parasitic elements has been proposed. Generally, generating a band rejection behaviour is based on shifting the antenna impedance in order to obtain a mismatch at a particular frequency. In this work, instead of performing the transaction from a wide single band antenna into a multiband antenna, we propose to transform a multiband antenna into a single operating band using a low cost method. Firstly, the performance of a compact multiband printed antenna is investigated in Section 2, then band rejection features are etched on the antenna resulting in four variants of the antenna design, which are detailed in Section 3. CST Microwave Studio was used to obtain the simulation results such as radiation patterns, gain, and reflection coefficients.

Received 31 July 2016, Accepted 21 September 2016, Scheduled 12 October 2016

* Corresponding author: Lamyae Akrou (aklamyae@gmail.com).

[1] Faculty of Science, Abdelmalek Essaadi University, Tetouan, Morocco. [2] Institute of Telecommunications, Departamento de Engenharia Eletrotécnica e de Computadores, University of Coimbra, Coimbra, Portugal. [3] National School of Applied Sciences, Abdelmalek Essaadi University, Tetouan, Morocco. [4] National School of Computer Science and Systems Analysis Mohamed V-Souissi, Rabat, Morocco.

2. MULTIBAND ANTENNA DESIGN

The proposed antenna has a rectangular ring shape, with a compact size (24 mm × 18 mm) and a uniform strip width $w_d = 2$ mm. The antenna is printed on an FR-4 dielectric substrate, with a thickness of 1.6 mm and relative permittivity (ε_r) of 4.4. The microstrip feed line used to feed the antenna is offset from the center, with a width w_f fixed to 2.89 mm providing the antenna with an input impedance of 51.95 Ω. Moreover, partial ground plane is used to obtain a broadened impedance bandwidth. The antenna design shows multiple resonances over a wide range of frequency (3–38 GHz). Fig. 1 depicts the described structure. The optimized values of the antenna parameters are shown in Table 1.

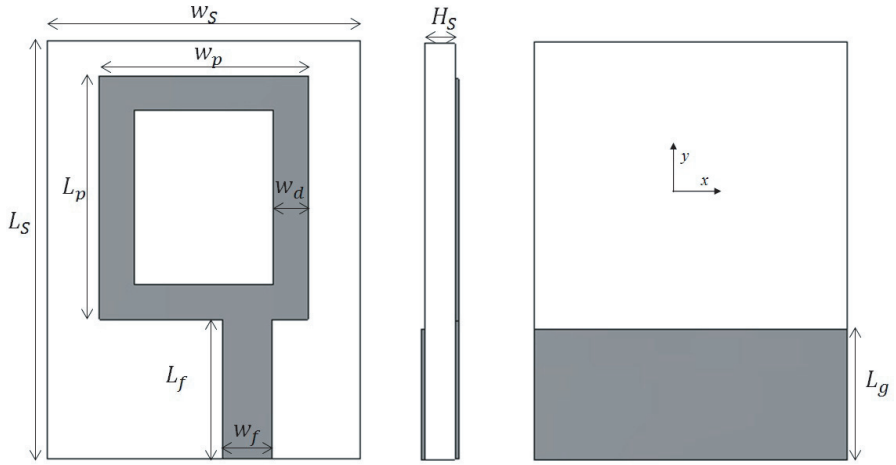

Figure 1. Initial multiband antenna design.

Table 1. Optimized parameters for the proposed antenna.

Parameter	Value (mm)
w_s	18
L_s	24
H_s	1.6
w_p	12
L_p	14
w_d	2
w_f	2.89
L_f	8
L_g	7.5

The simulated antenna demonstrates a good tetra band performance, with a lower $|S_{11}|$, which indicates that the antenna has a good efficiency. The antenna has four operating wide bands with respect to the −10 dB bandwidth convention, given as: [3.88–5.4 GHz], [7.4–11.24 GHz], [12–16.52 GHz], and [22.28–36.4 GHz], respectively. Fig. 2 presents the reflection coefficient of the simulated multiband antenna compared with its measured data. Good results were obtained, where the difference seen between the simulated and measured reflection coefficient might be due to the use of an SMA port to perform the measurements instead of an SMK port, as no appropriate SMK port was found in the market. Fig. 3 shows the simulated input impedance, real and imaginary parts, which are used to deduce the operational characteristics of the antenna at resonance, and to build an equivalent circuit model of the antenna. Accordingly, a lumped element model is proposed using a second order circuit

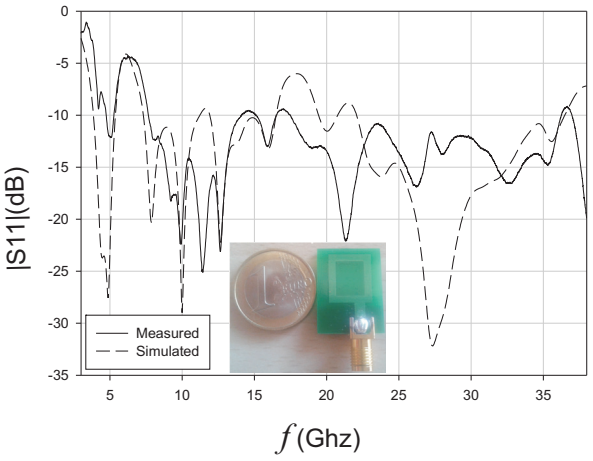

Figure 2. The reflection coefficient of the proposed antenna design.

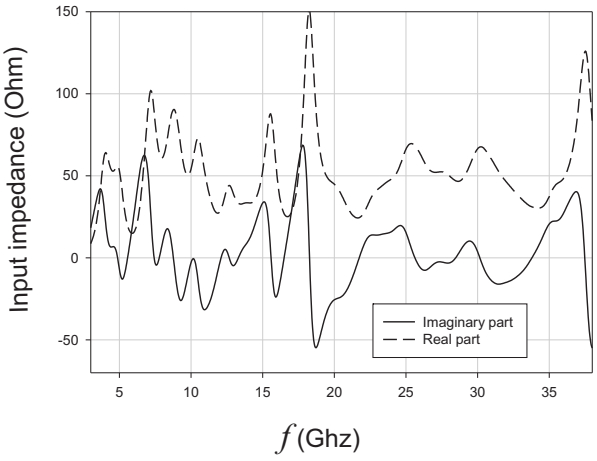

Figure 3. Z parameters of the reference antenna.

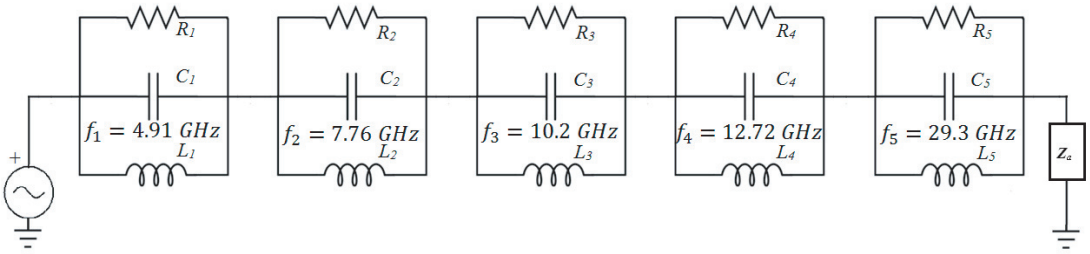

Figure 4. Equivalent circuit model for the proposed antenna, $R_1 = 52.29\,\Omega$, $L_1 = 0.689\,\text{nH}$, $C_1 = 1.989\,\text{pF}$, $R_2 = 64.36\,\Omega$, $L_2 = 0.272\,\text{nH}$, $C_2 = 1.545\,\text{pF}$, $R_3 = 57.31\,\Omega$, $L_3 = 0.03\,\text{nH}$, $C_3 = 0.666\,\text{pF}$, $R_4 = 42.74\,\Omega$, $L_4 = 0.19\,\text{nH}$, $C_4 = 0.823\,\text{pF}$, $R_5 = 45.51\,\Omega$, $L_5 = 0.122\,\text{nH}$, $C_5 = 0.24\,\text{pF}$.

with two independent energy storage elements (inductors and capacitors). The proposed circuit model presented in Fig. 4 is composed from a cascade of parallel RLC circuits using resistors (R_i), inductors (L_i), and capacitors (C_i), for $i = 1, 2, \ldots, 5$, terminated by an impedance load of $50\,\Omega$. The initial values of R_i are taken from the real part of the input impedance curve in Fig. 3 at the resonance frequencies determined as the imaginary part curve crosses the zero impedance axis. The initial values for L_i and C_i components were obtained using the given expressions [5]:

$$L_i = \frac{R_i}{2\pi f_{r_i} Q_i} \tag{1}$$

$$C_i = \frac{1}{(2\pi f_{r_i})^2 Q_i} \tag{2}$$

$$Q_i = \frac{f_{r_i}}{f_u - f_l} \tag{3}$$

where f_{r_i} is the resonance frequency; Q_i is the quality factor; f_u and f_l are the upper and lower frequencies, respectively, of each operating band. The final values of the lumped elements are obtained after tuning the circuit elements. The reflection coefficient of the reference antenna and of the proposed equivalent circuit model are compared in Fig. 5. A good agreement between resonances is observed, over almost all the operating bands, with a small shifting in bandwidth for the Ku-band due to the closeness between the resonance frequencies of the operating bands, namely [7.4–11.24 GHz], and [12–16.52 GHz]. Analytically, the bandwidth of each of the RLC parallel components (BW_{parallel_i}) can be

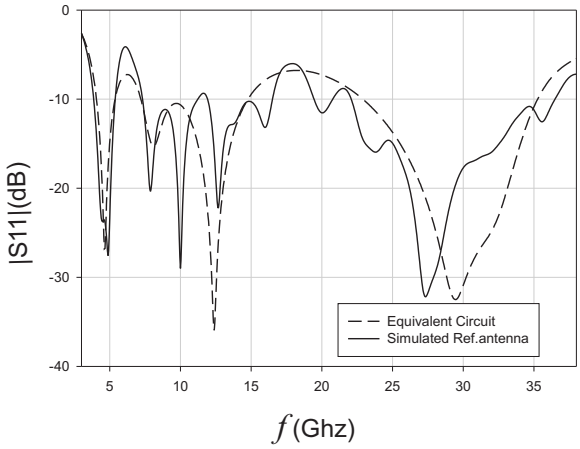

Figure 5. The reflection coefficient of the simulated reference multiband antenna and its equivalent circuit.

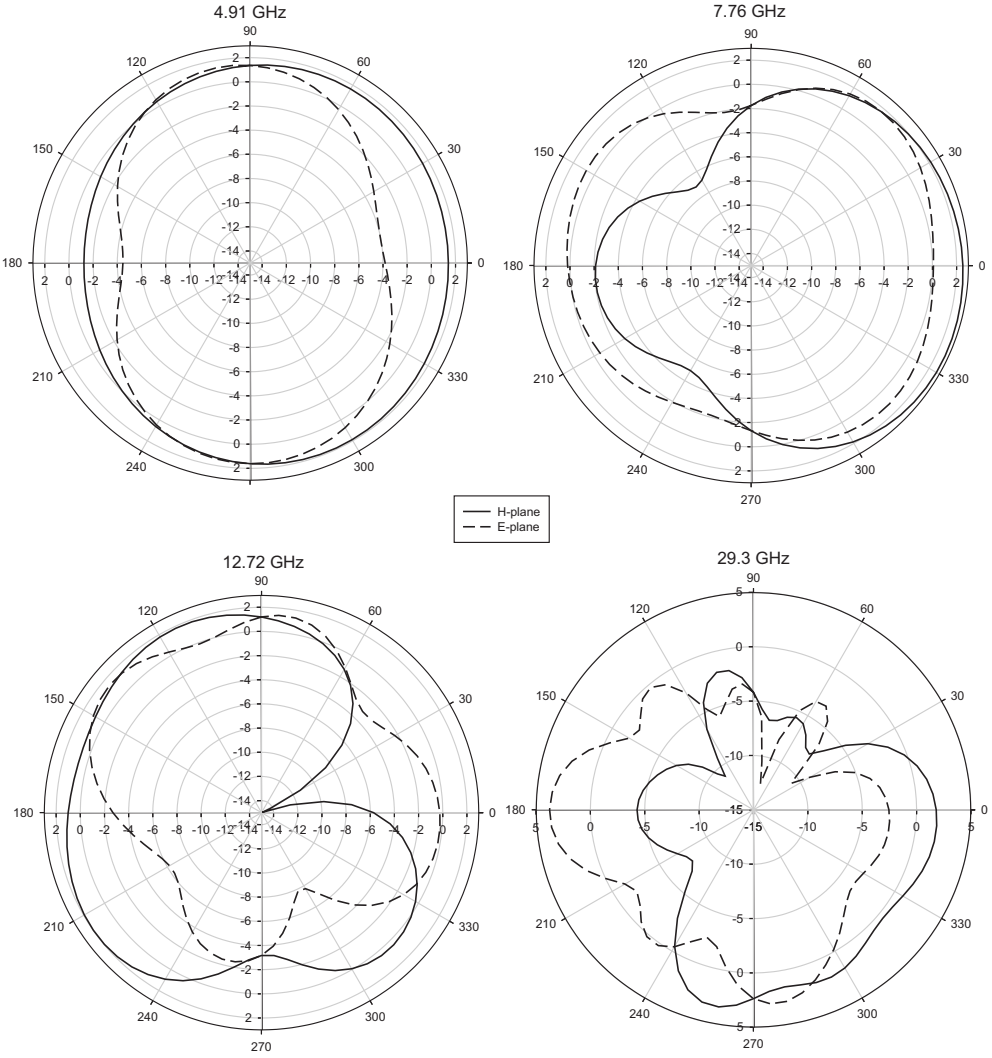

Figure 6. Radiation patterns of the reference antenna in the E (XZ) and H (XY)-planes for 4.91 GHz, 7.76 GHz, 12.72 GHz and 29.3 GHz.

expressed using R_i and C_i [4].

$$BW_{\text{parallel}_i} = \frac{1}{R_i C_i} \tag{4}$$

Regarding the radiation performance of the reference antenna, Fig. 6 illustrates the obtained radiation patterns at several frequencies. It is observed that the proposed antenna behaves as a monopole antenna at 4.91 GHz, while a wide radiation pattern covering almost all the azimuth range is obtained at 7.76 GHz, 12.72 GHz and 29.3 GHz, respectively. For the 3 dB beamwidth in the elevation plane, high values are found for 7.76 GHz, 12.72 GHz, and 29.3 GHz, with 176°, 115.4°, and 43.3°, respectively. In terms of the antenna gain and efficiency, very satisfactory performance is achieved (see Fig. 7), with a gain range varying between 2.033 dBi and 7.77 dBi, and a radiation efficiency above 84% for all the operating bands.

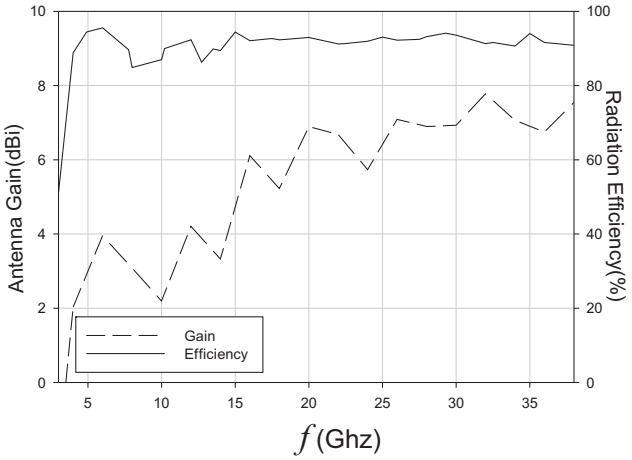

Figure 7. Gain and Radiation efficiency of the reference antenna.

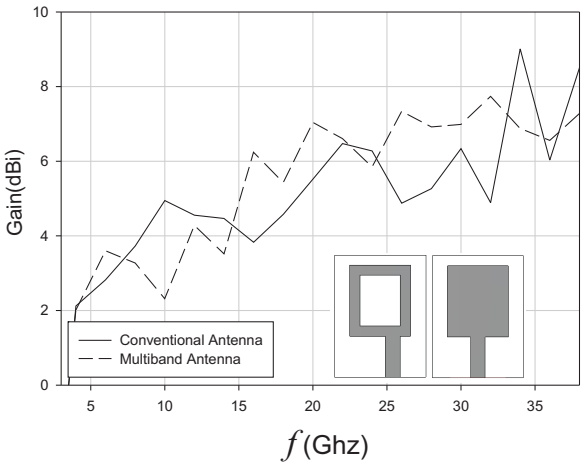

Figure 8. Gain comparison between the multiband antenna and the conventional UWB antenna.

The antenna performances were also compared with a conventional rectangular UWB antenna. The same antenna dimensions were kept during the simulation including the partial ground plane. Fig. 8 demonstrates that the overall gain of the multiband antenna is improved compared with the known UWB antenna structure, with an average gain of 6 dBi over the operating frequency band.

3. BAND REJECTION METHODS

In order to add the band rejection features to the reference antenna, slots and parasitic elements are used. The surface current distributions of the reference antenna is depicted in Fig. 9 for the resonance frequencies, i.e., 4.91 GHz, 7.76 GHz, 12.72 GHz and 29.3 GHz. It can be observed that higher surface current distribution is reached on the feed line and at its proximity on the antenna strip, also on the non radiating edges and within the ground plane. Based on that, the notch elements placements are chosen to be embedded in the partial ground plane, precisely in the coupled microstrip-ground area.

3.1. Ku-Band Antenna

This section will make use of the slotted antenna scheme in order to add the band rejection properties to the multiband antenna, as it has been proved in [11] that embedding spur lines on the radiating element can excite a new resonant mode. In this work, it is found that etching spur lines in the ground plane can provide band rejection at the desired frequency. The proposed antenna design is modified in order to operate in the Ku-band while rejecting the other coexisting bands. The modified antenna is

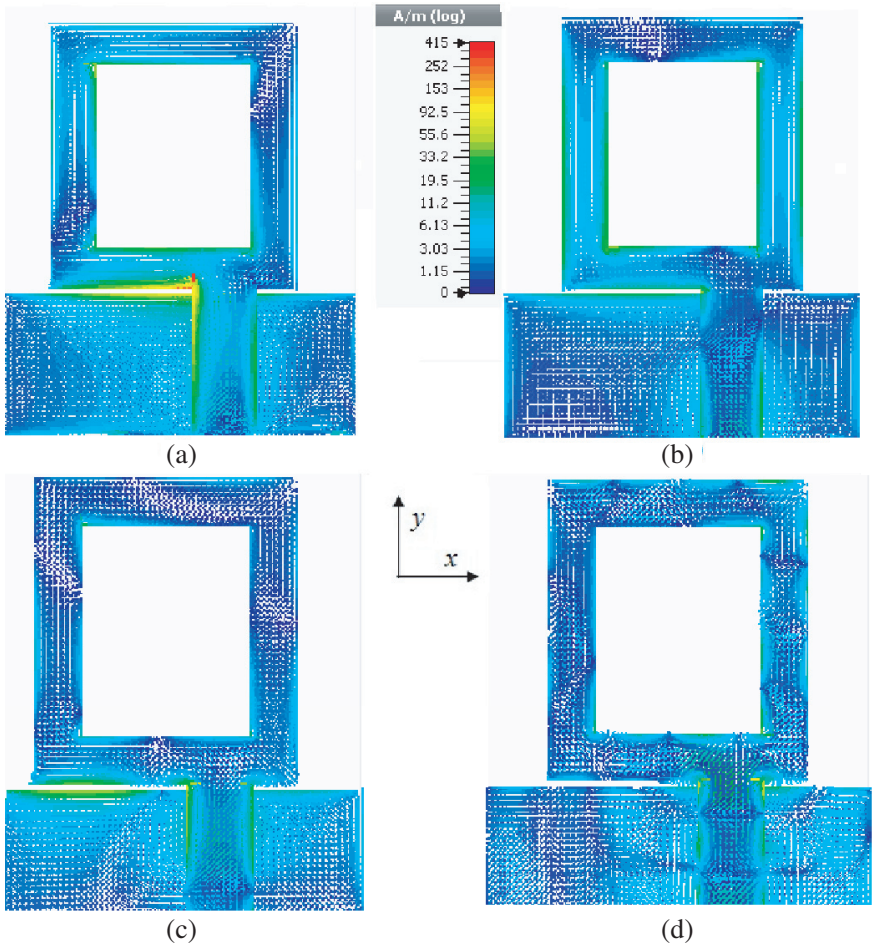

Figure 9. Surface current distribution on the reference multiband antenna at (a) 4.91 GHz, (b) 7.76 GHz, (c) 12.72 GHz and (d) 29.3 GHz.

presented in Fig. 10, where a spur line has been cut from the ground plane to reject the first operating band [3.88–5.4 GHz], and its length is approximately around quarter wavelength at the first resonance (4.91 GHz). Further, a T-shaped slot is used as a band stop filter along the Ka-band. Therefore, the slot length is adjusted to be around half wavelength of the unwanted frequency 29.3 GHz. The resonance of the spur line is calculated using Eq. (5):

$$f_r = \frac{\sqrt{2} \times c}{\lambda\sqrt{\varepsilon_r + 1}} \tag{5}$$

where f_r is the resonance frequency, ε_r the relative dielectric constant, c the speed of light in vacuum, and λ the wavelength of the slot/spur line which is considered to be:

$$\lambda = A \times L \tag{6}$$

where A is a constant equal to 4 when a quarter wavelength is considered and set to 2 when a half wavelength slot/spur line is used. Here, L stands for the spur line/slot length. When the spur line is considered, L is:

$$L = s_1 + d + w \tag{7}$$

while for the T-shaped slot L is:

$$L = s_2 + d + w \tag{8}$$

where s_1 and s_2 represent the lengths of the longitudinal slots, adjusted to 7.32 mm and 2.7 mm, respectively, after simulating the design. d is the distance from the top edge of the partial ground, and

w is the width of the slots/spur line fixed to 0.3 mm. Fig. 9(a) shows a high surface current distribution extended along a wide area in the ground plane given rise to multiple choices of the placement of the longitudinal slot s_1 of the spur line. Hence, the effect of the distance d of s_1 from the top edge of the ground is examined in Fig. 11. Parameter d is fixed to 0.8 mm as its corresponding curve results in a return loss above −10 dB for the rejected bands. Moreover, the effect of distance w_f between the two etched elements is presented in Fig. 12, where the parameter value of w_f for this design is set to 2.2 mm, as it gives good performance. It is worth mentioning that although the design is proposed for the Ku-band, the operating band of this antenna design includes the C and X-bands, which is mainly due to the closely spaced wavelengths of these bands. Otherwise, this proposed antenna design shows a wide bandwidth ranging between 7.78 GHz and 15.869 GHz, with a low return loss, and good band rejection performance for the rest of the examined frequency range (see Fig. 13).

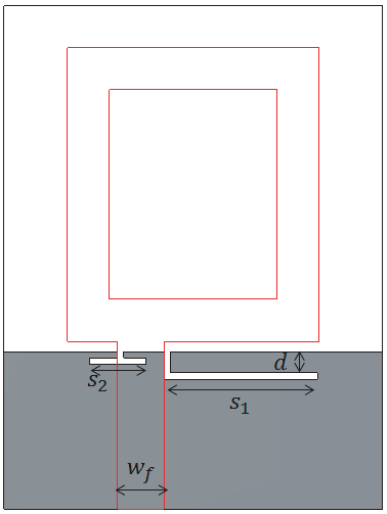

Figure 10. Back view of the proposed Ku-band antenna with the embedded slot and spur line (red lines illustrates the positioning of the front view with respect to the ground plane).

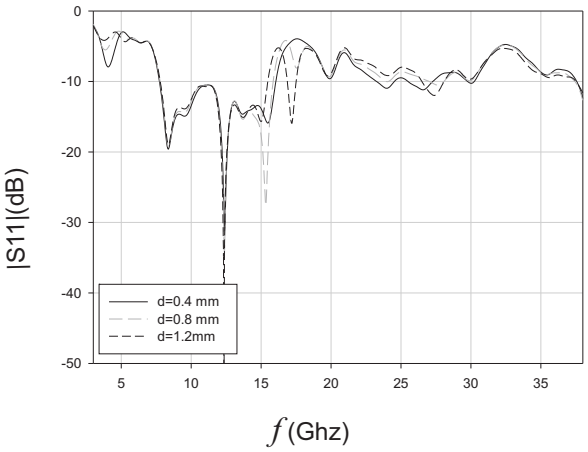

Figure 11. Comparison of the simulated reflection coefficient for different values of the distance d.

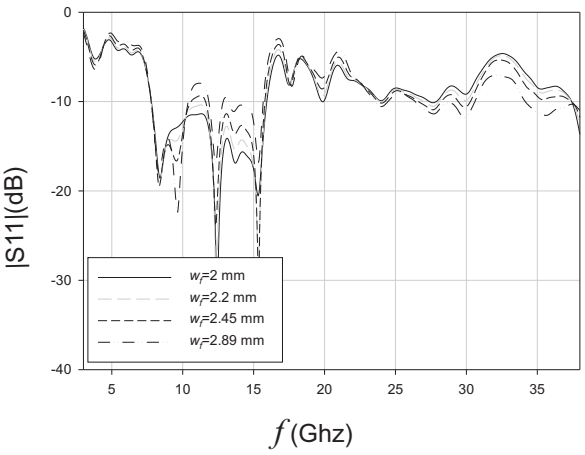

Figure 12. Comparison of the reflection coefficient parameter for different values of the feed line width w_f.

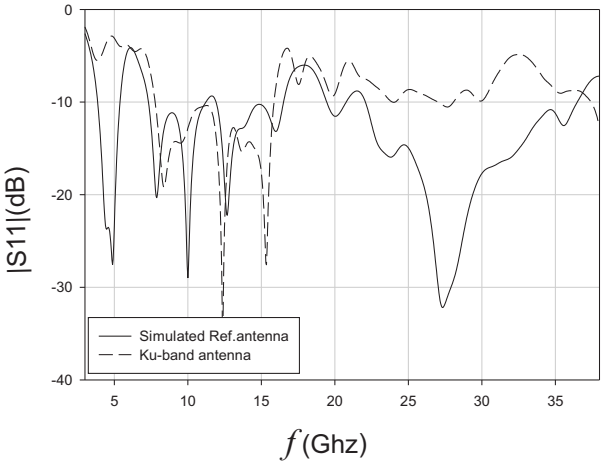

Figure 13. Simulated reflection coefficient of the proposed Ku-band antenna and the reference antenna.

3.2. Ka-Band Antenna

In this section, a modified antenna design operating within the Ka-band [26.5 GHz–40 GHz] is proposed. For this design, all the reference antenna parameters are kept unchanged. Fig. 14 shows the modified design, with two spur lines etched on the ground plane, and each one has a width of 0.3 mm. The longitudinal slot s_1 of the spur line is used to reject the first operating band, with a length adjusted to be approximately equal to the quarter wavelength ($\simeq 7.32$ mm) at 4.91 GHz, and s_2 is embedded in order to exclude the C, X and Ku bands, with a length also equal to the quarter wavelength ($\simeq 4.5$ mm) at 7.76 GHz, with an open ended vertical slot l_1 (2.38 mm $\times$ 0.3 mm) etched in between. Slots s_1 and s_2 create a predominance storing of magnetic energy at the short ends of the slots producing an inductive reactance, while the open ends of the spur lines or of the slot are responsible for radiation. The addition effect of each element is illustrated in Fig. 15. The proposed antenna shows good results, wide single operating bandwidth from 22.77 GHz to 37 GHz, and a triple band-rejection feature with a reduced return loss within the working band in Fig. 16.

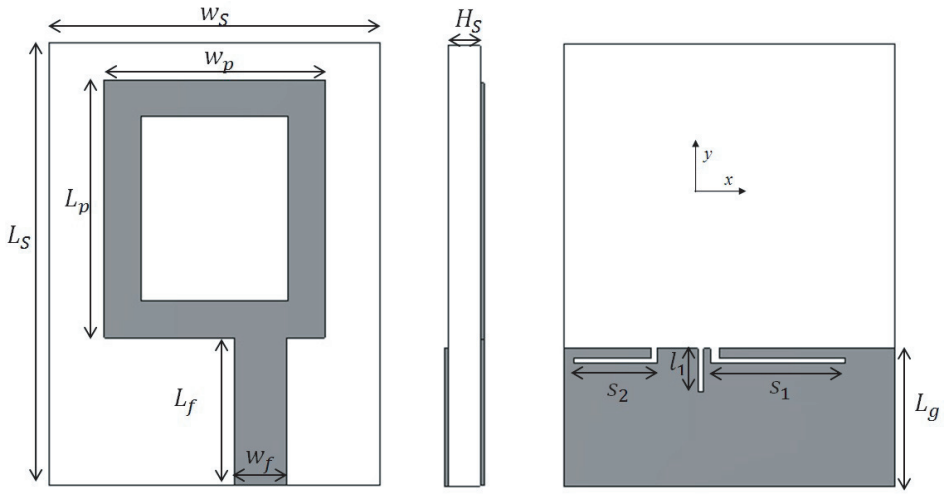

Figure 14. Ka-band patch antenna including the spur lines and an open ended slot.

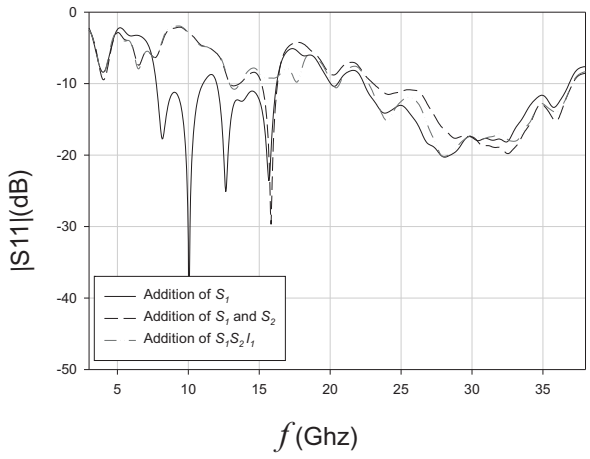

Figure 15. The simulated reflection coefficients of the proposed Ka-band antenna during its development.

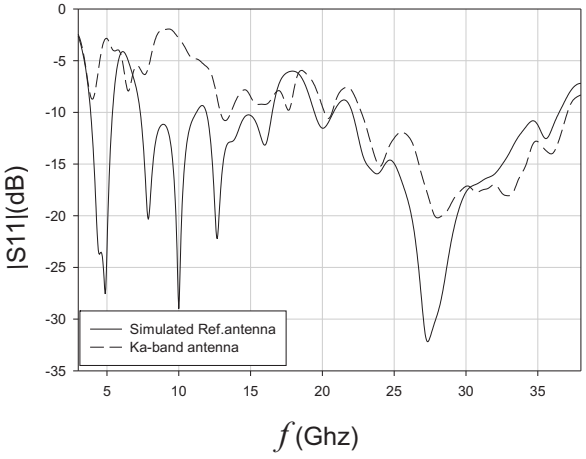

Figure 16. The simulated reflection coefficients of the proposed Ka-band antenna and the reference antenna.

3.3. Parasitic Antenna Design

In this part of the work, the addition of a parasitic element is investigated. The proposed geometry is shown in Fig. 17. An L-shaped arm is capacitively coupled to the radiating element, spacing a set to 0.3 mm. The arm is formed by joining two strips L_{p1} (= 14.75 mm) and L_{p2} (= 2.88 mm) with width w (= 0.5 mm). The embedded L-shaped arm location is chosen based on the obtained surface current distribution at 4.91 GHz shown in Fig. 18. This arrangement causes the current distribution on the parasitic element to be out of phase with that on the radiating element, so that the added arm can produce a band rejection feature at the desired frequency. Thus, as seen from Fig. 18(a), a higher surface current distribution is mainly concentrated near the L-shaped arm, where the currents are oppositely directed between the parasitic arm and the antenna [12]. The effect of the added parasitic element can

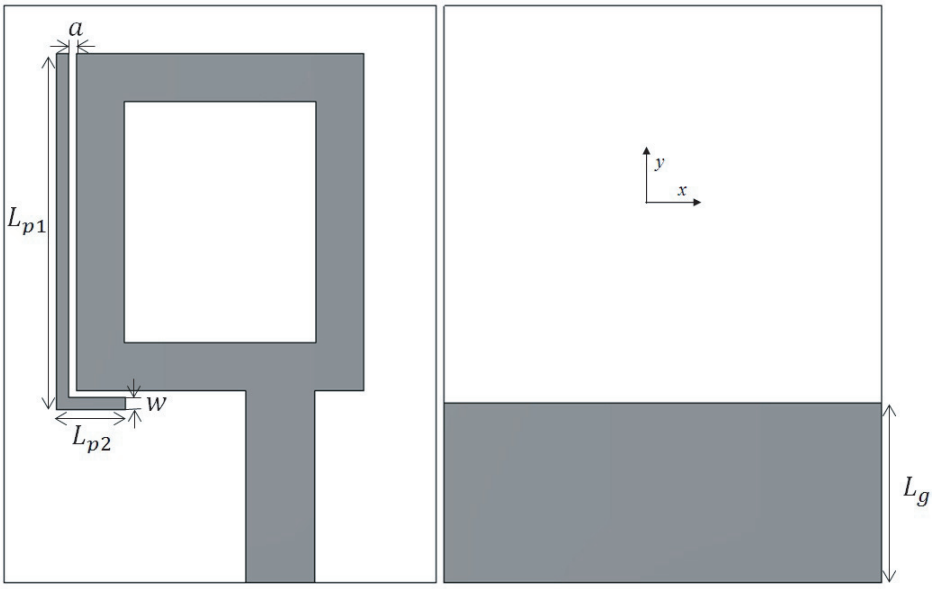

Figure 17. The modified antenna with an L-shaped parasitic element.

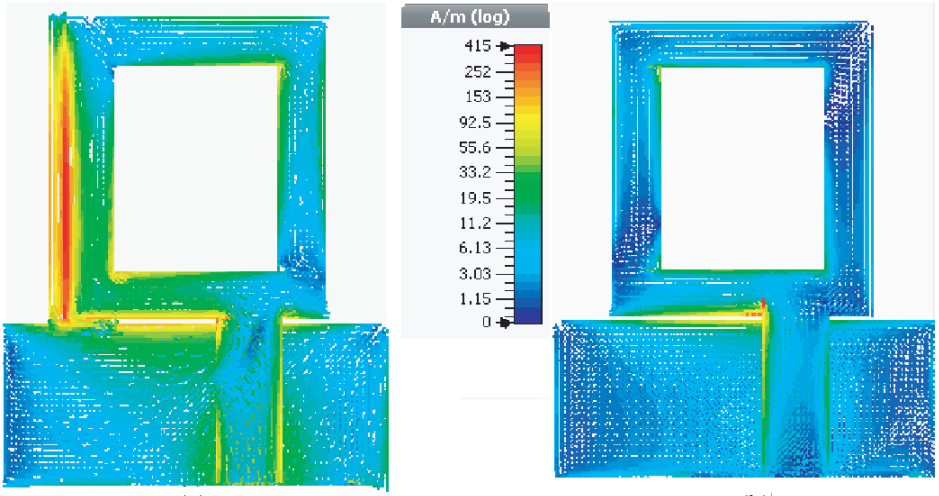

Figure 18. The surface current distribution at the unwanted frequency 4.91 GHz for (a) the modified antenna, (b) reference antenna.

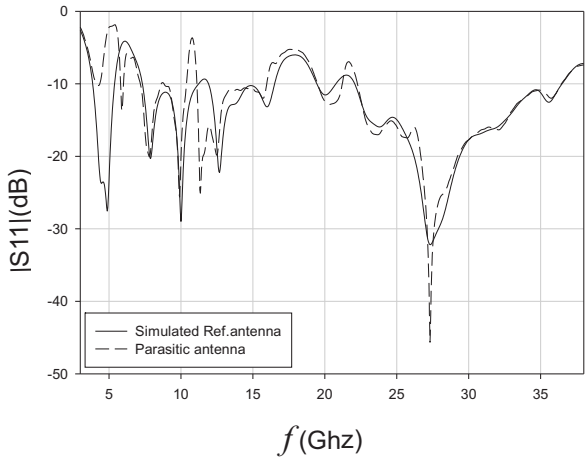

Figure 19. The simulated reflection coefficients of the parasitic antenna compared with the reference antenna.

be seen from Fig. 19, where the reflection coefficient is above −10 dB for the first band [3.88–5.4 GHz], almost without affecting the rest of the operating bands. Accordingly, the proposed antenna has a band-stop-filter-like response for Wireless Local Area Network (WLAN), Worldwide interoperability for Microwave Access (WiMAX), and the 5 GHz U-NII systems.

3.4. Open Square Ring Antenna Design

In this section, band rejection features are implemented using the Open Square Ring structure by etching a gap along the feed line and going through the antenna. Fig. 20 illustrates the proposed antenna design. An examination of the key parameters effects, w_{gap} and L_{gap}, is performed. The obtained results are presented in Fig. 21 and Fig. 22, where the L_{gap} values are taken to be approximately equal to the quarter wavelengths at 4.91 GHz, 7.76 GHz, and 10.2 GHz, respectively. The other wavelengths of 12.72 GHz and 29.3 GHz are tested but not shown in the plot for clarity purpose only, as the same deductions are

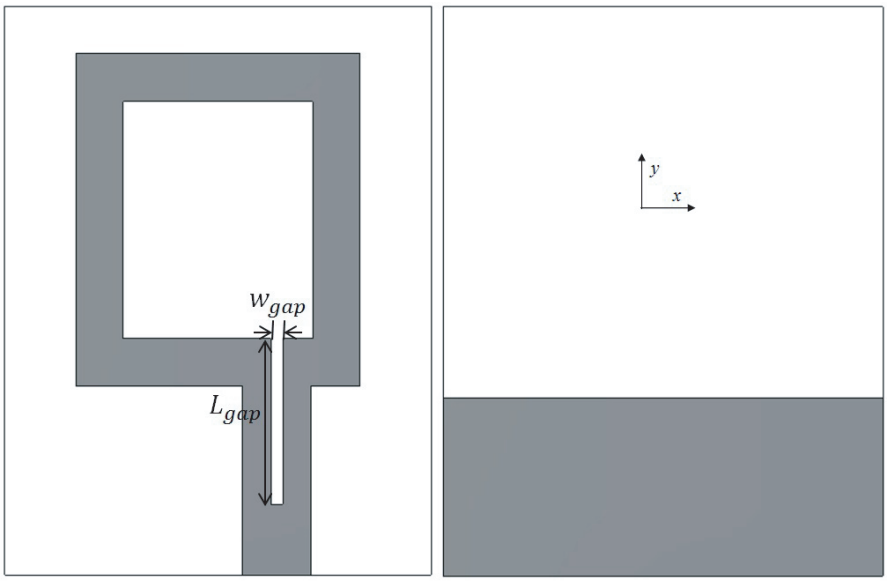

Figure 20. The proposed antenna structure using the Open Square Ring design.

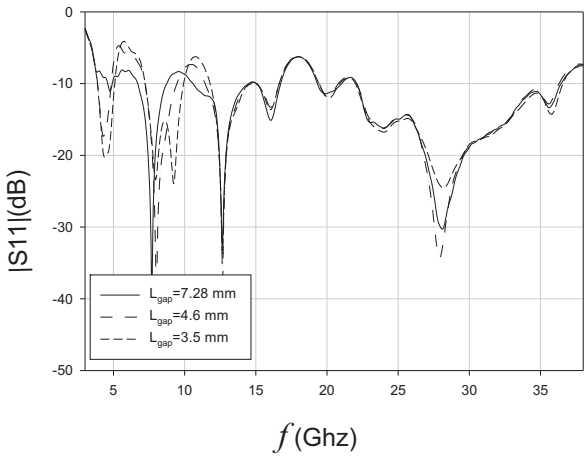

Figure 21. The simulated reflection coefficients of the Square Open Ring antenna for various lengths of the gap.

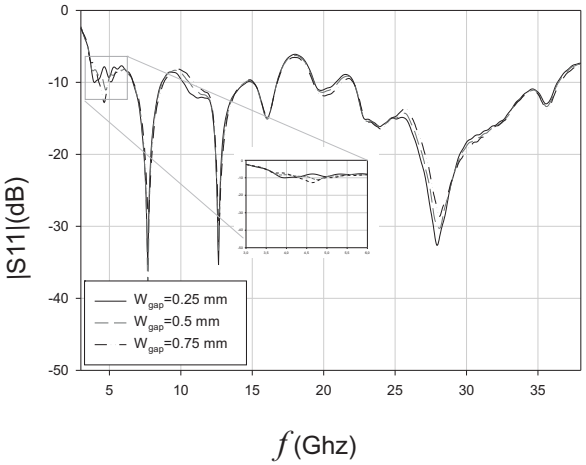

Figure 22. The simulated reflection coefficients of the Square Open Ring antenna by varying the gap width with L_{gap} fixed to 7.28 mm.

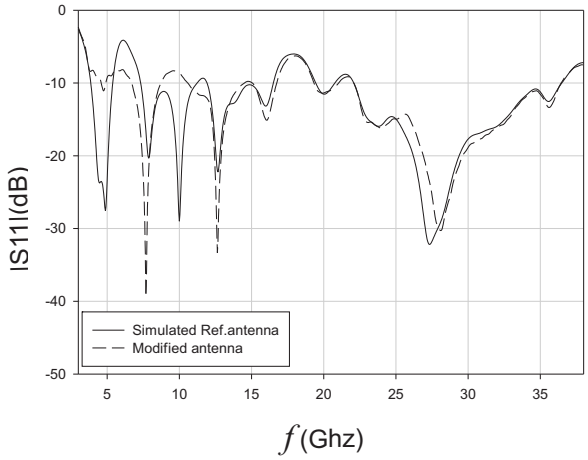

Figure 23. The simulated reflection coefficients of the proposed Open Square Ring antenna compared with the reference antenna.

obtained. It is observed that the reflection coefficient decreases as the wavelength decreases and that as the gap width increases the gap loses its band rejection feature accordingly. Thus, the proposed antenna preserves the same behaviour as the reference antenna over all the operating range, except along the first operating band, as can be seen from Fig. 23, for $L_{gap} = 7.28$ GHz which is quarter wavelength of 4.91 GHz and w_{gap} set to 0.5 mm for feasibility of the design.

4. CONCLUSION

Firstly, this work presents a compact multiband antenna design for land mobile satellite communications use, precisely for vehicles. The proposed antenna with a simple design can operate simultaneously in four bands providing several applications within bands such as WLAN, WiMAW, 5 GHz U-NII, C-band, X-band, Ku-band, K-band and Ka-band. A conceptual equivalent circuit model of the antenna is also proposed. Stable radiation patterns, and high efficiency and gain over the operating bandwidths are achieved with a peak value of 7.77 dBi. Secondly, four derived designs are proposed to provide interference avoidance and band rejection features, which is achieved by etching spur lines and slots

on the ground plane for the two first proposed designs, resulting in two single band antennas with a wide impedance bandwidth. The two other designs are obtained by acting on the radiating element shape and by placing an L-shaped parasitic element at the vicinity of the antenna. The designs provide good band-rejection filter response for the rejected bands, with a lower reflection coefficient in bands of interest.

REFERENCES

1. Balanis, C. A., *Antenna Theory, Analysis and Design*, 3rd Edition, John Wiley & Sons, 2005.
2. Garg, R., *Microstrip Antenna Design Handbook*, Artech House, 2001.
3. Nguyen, T. D., D. H. Lee, and H. C. Park, "Design and analysis of compact printed triple band-notched UWB antenna," *IEEE Antennas and Wireless Propagation Letters*, Vol. 10, 2011.
4. Zhu, F., S. Gao, A. T. S. Ho, R. A. Abd-Alhameed, C. H. See, T. W. C. Brown, J. Li, G. Wei, and J. Xu, "Multiple band-notched UWB antenna with band-rejected elements integrated in the feed line," *IEEE Transactions on Antennas and Propagation*, Vol. 61, No. 8, August 2013.
5. Ma, T.-G., R.-C. Hua, and C.-F. Chou, "Design of a multiresonator loaded band-rejected ultrawideband planar monopole antenna with controllable notched bandwidth," *IEEE Transactions on Antennas and Propagation*, Vol. 56, No. 9, September 2008.
6. Dong, Y. D., W. Hong, Z. Q. Kuai, and J. X. Chen, "Analysis of planar ultrawideband antennas with on-ground slot band-notched structures," *IEEE Transactions on Antennas and Propagation*, Vol. 57, No. 7, July 2009.
7. Zhu, F., S. Gao, A. T. S. Ho, C. H. See, R. A. Abd-Alhameed, J. Li, and J. Xu, "Dual band-notched tapered slot antenna using $\lambda/4$ band-stop filters," *IET Microwaves, Antennas & Propagation*, Vol. 6, No. 15, 1665–1673, 2012.
8. Tang, M.-C., H. Wang, T. Deng, and R. W. Ziolkowski, "Compact planar ultrawideband antennas with continuously tunable, independent band-notched filters," *IEEE Transactions on Antennas and Propagation*, Vol. 64, No. 8, August 2016.
9. Choi, N., C. Jung, J. Byun, F. J. Harackiewicz, M.-J. Park, Y.-S. Chung, T. Kim, and B. Lee, "Compact UWB antenna with I-shaped band-notch parasitic element for laptop applications," *Antennas and Wireless Propagation Letters*, Vol. 8, 2009.
10. Jung, J., H. Lee, and Y. Lim, "Compact band-notched ultra-wideband antenna with parasitic elements," *Electronics Letters*, Vol. 44, No. 19, 2008.
11. Wong, K.-L., *Compact and Broadband Microstrip Antennas*, Technology & Engineering, 344 pages, John Wiley & Sons, April 7, 2004.
12. Balalem, A., A. R. Ali, J. Machac, and A. Omar, "Quasi-elliptic microstrip low-pass filters using an interdigital DGS slot," *IEEE Microw. Wireless Compon. Lett.*, Vol. 17, No. 8, August 2007.